

We are IntechOpen, the world's leading publisher of Open Access books Built by scientists, for scientists

4,800

Open access books available

122,000

International authors and editors

135M

Downloads

Our authors are among the

154

Countries delivered to

TOP 1%

most cited scientists

12.2%

Contributors from top 500 universities



WEB OF SCIENCE™

Selection of our books indexed in the Book Citation Index
in Web of Science™ Core Collection (BKCI)

Interested in publishing with us?
Contact book.department@intechopen.com

Numbers displayed above are based on latest data collected.
For more information visit www.intechopen.com



Advanced Monitoring of Wind Turbine

*Steve Alan Talla Ouambo, Alexandre Teplaira Boum
and Adolphe Moukengue Imano*

Abstract

This chapter presents a general framework for the doubly fed induction generator (DFIG). We apply and analyze the behavior of three estimation techniques, which are the unscented Kalman filter (UKF), the high gain observer (HGO) and the moving horizon estimation (MHE). These estimations are used for parameters estimation of the doubly fed induction generator (DFIG) driven by wind turbine. A comparison of those techniques has been made under different aspects notably, computation time and estimation accuracy in two modes of operation of the DFIG, the healthy mode and the faulty mode. The performance of the MHE has been clearly superior to other estimators during our experiments. These estimation tools can be used for monitoring purposes.

Keywords: doubly-fed induction generator, high gain observer, unscented Kalman filter, moving horizon estimation, parameters estimation, monitoring

1. Introduction

Nowadays most of generated electricity comes from nonrenewable sources of fuel. These products transfer to the atmosphere important quantities of CO₂, and inescapably leading to the warming up of the atmosphere [1]. The production of the wind energy spreads through the world, and significantly, it imposed itself during the past decade [2]. Doubly-fed induction generators (DFIGs) are actually the most used wind power generators in many countries [3].

Therefore, many contributions have been made to the inverters and converters usually in DFIG used in the power electronics domain [4]. A doubly fed induction generator model for transient stability analysis has been proposed in [5], in which authors focused their study on the control loops of instantaneous response. In [6], authors have been proposed some robust observers to estimate states and actuator faults for different class of linear and nonlinear systems at the same instant. Though systems are becoming more and more complex, DFIG can be subject by many types of faults [7], diagnosis and faults estimation issues have become primordial to ensure a good supervision of systems and guarantee the safety of materials and operators (humans) [8].

A survey based on current sensor fault detection and isolation and control reconfiguration current for doubly fed induction generator has been proposed by [9]. Studies led by [10], have contributed to an adaptive parameter estimation algorithm used for estimating the rotor resistance of the DFIG, however, the others

parameters were assumed to be constant. To improve the extended Kalman filter (EKF), a new nonlinear filtering algorithm named the unscented Kalman filter (UKF) has been developed in [11]. Widely used in some fields, UKF has been found in several studies such as training of neural networks [12], multi-sensor fusion for instance.

This chapter investigates the usage of the unscented Kalman filter UKF, high gain observer (HGO) and the moving horizon estimator (MHE) to estimate the dynamic states and electrical parameters of the wind turbine system. These estimates can be used to enhance the performance of doubly fed induction generator in power systems, for rotor and stator resistances faults in the circumstances where internal states will be involved in a control design [3] and the acquisition of internal states, which are relatively difficult to get can realized from the dynamic state estimation and for monitoring purposes. The chapter is organized as follows: in Section 2, the mathematical model for DFIG is presented, followed by the description of estimation algorithms in Section 3. The results of the parameter estimation tests are presented in Section 4. Finally Section 5 gives the conclusions.

2. Mathematical model for DFIG

In this section, we deal with the mathematical modeling of the DFIG-based wind energy system, we will only describe the wind turbine (also called drive train), and the asynchronous generator (also called induction generator) because this chapter focuses on estimating of the parameters and dynamic states of the DFIG **Figure 1**. Two frames of reference are used in this model: stator voltage (d-q) reference frame and mutual flux (d-q) reference frame. In **Tables 1** and **2**, all parameters and constants are given.

2.1 Modeling of the wind turbine

From the wind, the power extracted can give the mechanical torque. The energy from the wind is extracted from the wind turbine and converted into mechanical power [14]. The wind turbine model is based on the output power characteristics, as Eqs. (1) and (2), [15].

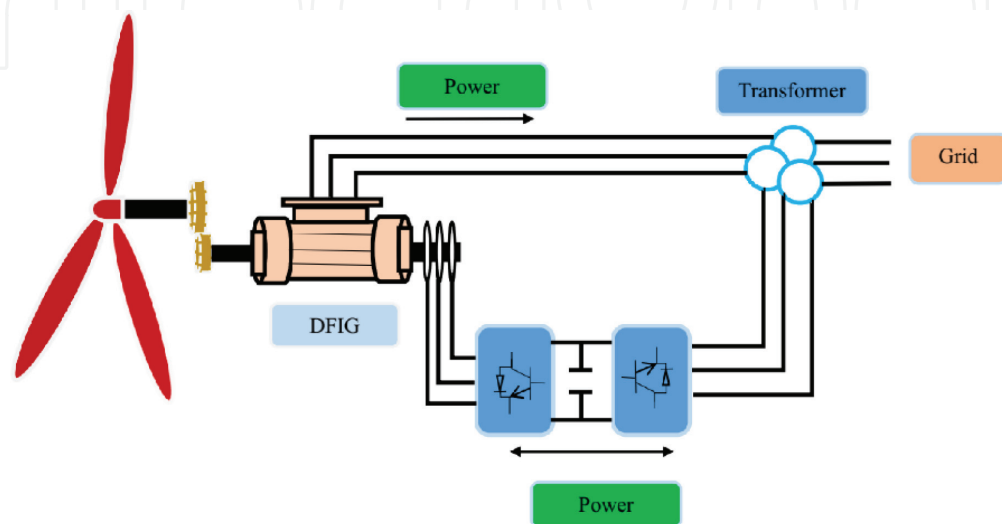


Figure 1.
Configuration of DFIG-based wind turbine system [13].

Parameters	Values
Rated active power (Ps)/(MW)	1.5
Rated voltage (line to line) (Vs)/(V)	575
Rated DC-link voltage (Vdc)/(V)	1200
Number of poles	4
Frequency (f)/(Hz)	60
Stator resistance (Rs)/(pu)	0.00707
Rotor resistance (Rr)/(pu)	0.005
Stator leakage inductance (Ls)/(pu)	0.171
Rotor leakage inductance (Lr)/(pu)	0.156
Magnetizing inductance (Lm)/(pu)	2.9
DC-link capacitance (C)/(F)	0.04

Table 1.
 Parameters of the DFIG.

Parameters	Values
Rated wind speed (v_w)/(m s ⁻¹)	12
Number of blade	3
Radius of blade (R)/m	35.25
Gearbox gain (G)	91
Moment of inertia (J_{eq})/(kg m ²)	1000
Viscosity factor (f_{eq})/(N m s rad ⁻¹)	0.0024

Table 2.
 Parameters of the wind turbine.

$$P_m = C_p(\lambda, \beta) \frac{1}{2} \rho A v_w^3 = C_p(\lambda, \beta) E_w \quad (1)$$

$$\lambda_{TS} = \frac{R\omega_t}{v_w} \quad (2)$$

where the aerodynamic extracted power is P_m , which depends on C_p , the efficiency coefficient, the air density ρ , the turbine swept area A , and the wind speed v_w . The kinetic energy contained in the wind at a particular wind speed is given by E_w . The blade radius and angular frequency of rotational turbine are R and ω_t , respectively. $C_p(\lambda; \beta)$ the efficiency coefficient depends on tip speed ratio λ_{TS} and blade pitch angle β , determines the amount of wind kinetic energy that can be captured by the wind turbine system [13]. $C_p(\lambda; \beta)$ can be described as:

$$C_p(\lambda, \beta) = 0.5 \left(\frac{116}{\lambda_i} - 0.4\beta - 5 \right) e^{-21/\lambda_i} \quad (3)$$

where

$$\frac{1}{\lambda_i} = \frac{1}{\lambda_{TS} + 0.08\beta} - \frac{0.035}{\beta^3 + 1} \quad (4)$$

2.2 Modeling of the asynchronous generator

For the induction generator, the Park model is the model that is commonly used [16]. After applying the synchronously rotating reference frame transformation to the stator and rotor fluxes equations of the generator, the following differential equations describe the dynamics of the rotor and stator fluxes [17]:

$$\begin{cases} \dot{\Phi}_{dr} = \omega_b (v_{dr} + (\omega_s - \omega_r)\Phi_{qr} - R_r i_{dr}) \\ \dot{\Phi}_{qr} = \omega_b (v_{qr} - (\omega_s - \omega_r)\Phi_{dr} - R_r i_{qr}) \\ \dot{\Phi}_{ds} = \omega_b (v_{ds} + \omega_s \Phi_{qs} - R_s i_{ds}) \\ \dot{\Phi}_{qs} = \omega_b (v_{qs} - \omega_s \Phi_{ds} - R_s i_{qs}) \end{cases} \quad (5)$$

where $\omega_s = 1$ is the synchronous angular speed in the synchronous frame and $\omega_b = 2\pi f$ rad/s is the base angular speed, with $f = 60$ Hz. With additional variables stator-rotor mutual flux Φ_{dm} and Φ_{qm} , rotor current i_{dr} and i_{qr} and stator current i_{ds} and i_{qs} can be expressed as:

$$\begin{cases} i_{dr} = \frac{\Phi_{dr} - \Phi_{dm}}{L_{lr}} \\ i_{qr} = \frac{\Phi_{qr} - \Phi_{qm}}{L_{lr}} \end{cases} \quad (6)$$

$$\begin{cases} i_{ds} = \frac{\Phi_{ds} - \Phi_{dm}}{L_{ls}} \\ i_{qs} = \frac{\Phi_{qs} - \Phi_{qm}}{L_{ls}} \end{cases} \quad (7)$$

where

$$\begin{aligned} \Phi_{dm} &= L_{ad} \left(\frac{\Phi_{dr}}{L_{lr}} + \frac{\Phi_{ds}}{L_{ls}} \right) \\ \Phi_{qm} &= L_{aq} \left(\frac{\Phi_{qr}}{L_{lr}} + \frac{\Phi_{qs}}{L_{ls}} \right) \end{aligned} \quad (8)$$

are the stator-rotor mutual flux.

Where constants L_{ad} and L_{aq} are the (d - q) mutual flux factors, expressed as:

$$L_{ad} = L_{aq} = \frac{1}{\frac{1}{L_m} + \frac{1}{L_{ls}} + \frac{1}{L_{lr}}} \quad (9)$$

The relationship between mechanical torque T_m , electrical torque T_e and rotor speed ω_r can be shown by the following differential equation,

$$\dot{\omega}_r = \frac{1}{2H} (T_m - T_e - F\omega_r) \quad (10)$$

where constant F is the friction factor and H is the generator inertia, and T_e , the electrical torque which can be expressed as:

$$T_e = \Phi_{ds} i_{qs} - \Phi_{qs} i_{ds} \quad (11)$$

These equations are derived in [4] and all parameters are defined in per unit based on the generator ratings and synchronous speed.

3. Estimation algorithms

3.1 High gain observer

This observer class is applied for nonlinear system classes of the form Eq. (12). Its applications are so large [18, 19]. We briefly present the developed survey in [20] that points up the synthesis of observers adapted to the observable nonlinear systems. Consider the following nonlinear system:

$$\begin{cases} \dot{x} = f(x) + g(x)u \\ y = h(x) \end{cases} \quad (12)$$

where $x \in R^n$, $u \in R^m$, $y \in R^s$.

First, the system Eq. (12) must be uniformly locally observable, and then it will be possible to make the variable change $z = \Gamma(x)$ that will transform the system Eq. (12) in the following form:

$$\begin{cases} \dot{z} = Az + \varphi(u, z) \\ y = Cz \end{cases} \quad (13)$$

The observer must satisfy the following theorem [20]:

- i. The function φ is globally Lipschitz uniformly to u .

Let $K = \begin{bmatrix} K_1 & & \\ & \ddots & \\ & & K_p \end{bmatrix}$ an adequate size matrix such as, for every K_i block, the

matrix.

$A_k - K_k C_k$ should give all its eigenvalues with negative real part:

Let's suppose that there exists two integer sets $\{\sigma_1, \dots, \sigma_n \in Z\}$ and $\{\delta_1 > 0, \dots, \delta_p > 0 \in N^*\}$ such as:

- ii. $\sigma_{\mu_k+v} = \sigma_{\mu_k+v-1} + \delta_r$, $k = 1, \dots, p$, $v = 1, \dots, \eta_k - 1$

- iii. $\frac{\partial \varphi_i}{\partial z_j} \neq 0 \Rightarrow \sigma_i \geq \sigma_j$, $i, j = 1, \dots, n$, $j \neq \mu_k$, $k = 1, \dots, p$

So,

$$\dot{\hat{z}} = A\hat{z} + \varphi(\hat{z}, u) - S_0^{-1}K(C\hat{z} - y) \quad (14)$$

is an exponential observer for the system Eq. (13) as well.

And there exists T_1 such as, for all T , $0 < T < T_1$.

With,

$$S(S, \delta) = \begin{bmatrix} S^{\delta_1} \Delta(S^{\delta_1}) & & \\ & \ddots & \\ & & S^{\delta_p} \Delta(S^{\delta_p}) \end{bmatrix}$$

$$\Delta_\theta(S) = \begin{bmatrix} 1 & & \\ & S & \\ & & \ddots \\ & & & S^{\eta_\theta-1} \end{bmatrix}$$

By operating a reverse variable change for coming back to the initial nonlinear system, the observer for the system Eq. (12) is given by:

$$\dot{\hat{x}} = f(\hat{x}) + g(\hat{x})u - \left(\frac{\partial \Gamma}{\partial \hat{x}}(\hat{x}(t)) \right)^{-1} S_{\theta}^{-1}(h(\hat{x}) - y) \quad (15)$$

\hat{x} : Estimated value of x .

Γ : An application $R^n \rightarrow R^n$.

With,

$$\Gamma = \left[h_1, L_f h_1, L_f^2 h_1, \dots, L_f^{\delta_1} h_1, h_2, L_f h_2, L_f^2 h_2, \dots, L_f^{\delta_2} h_2, \dots, h_p, L_f h_p, L_f^2 h_p, \dots, L_f^{\delta_p} h_p \right]^T$$

And $L_f^{\delta_k}$ is the Lie δ_k^i derivative.

P : Number of outputs.

And S_{θ} satisfies the following Lyapunov relation:

$$\dot{S} = -\theta S_{\theta} - A^T S_{\theta} - S_{\theta} A + C^T C = 0 \quad (16)$$

In [20], the demonstration is done.

3.2 The unscented Kalman filter

The unscented Kalman filter (UKF) has been essentially designed for the state estimation problems, and applied in some nonlinear control applications [11]. The unscented Kalman filter (UKF) compensates for approximation issues of the extended Kalman filter (EKF). A Gaussian random variable represents the state distribution, which is specified using a set of sample points chosen very carefully [12]. The unscented transformation (UT) is a method to estimate or calculate statistics of a random variable which is subjected to a nonlinear transformation [11]. In stochastic estimation problems, a common assumption usually is used which underline the fact that the process and measurement noise terms are additive, as in:

$$\begin{aligned} x_k &= f(x_{k-1}, u_{k-1}) + w_{k-1} \\ y_k &= h(x_k, u_k) + v_k \end{aligned} \quad (17)$$

The dimension of the sigma-points is the same as the state vector, that is to say $L = n_x$. The UKF is recursively executed, starting with the assumed initial conditions \hat{x}_0 and P_0 . First a set of sigma-points are generated from the prior state estimate \hat{x}_{k-1} and covariance P_{k-1} at each discrete-time step, as in:

$$\chi_{k-1} = \left[\hat{x}_{k-1} \quad \hat{x}_{k-1} + \sqrt{L + \lambda} \sqrt{P_{k-1}} \quad \hat{x}_{k-1} - \sqrt{L + \lambda} \sqrt{P_{k-1}} \right] \quad (18)$$

For the next point, each sigma point is passed through the state prediction function f that is nonlinear.

$$\chi_{k,k-1}^{(i)} = f\left(\chi_{k-1}^{(i)}, u_{k-1}\right), \quad i = 0, 1, 2, \dots, 2L \quad (19)$$

$\chi_{k,k-1}$ means that this is the predicted value of the sigma-point based on the information from the prior time step. Sigma-points transformed, the post transformation mean and covariance are computed using weighted averages of the transformed sigma-points [21],

$$\hat{x}_{k,k-1} = \sum_{i=0}^{2L} \eta_i^m \chi_{k,k-1}^{(i)} \quad (20)$$

$$P_{k,k-1} = Q_{k-1} + \sum_{i=0}^{2L} \eta_i^c \left(\chi_{k,k-1}^{(i)} - \hat{x}_{k,k-1} \right) \left(\chi_{k,k-1}^{(i)} - \hat{x}_{k,k-1} \right)^T \quad (21)$$

where $\eta_0^m = \lambda / (L + \lambda)$ and $\eta_0^c = \lambda / (L + \lambda) + 1 - \alpha^2 + \beta$. The measurement noise is also omitted from the observation function, as for the prediction as in:

$$\psi_{k,k-1}^{(i)} = h \left(\chi_{k,k-1}^{(i)}, u_k \right) \quad (22)$$

where is a matrix of output sigma-points. Output sigma-points are used to calculate output covariance matrix, the predicted output and cross-covariance by using:

$$\begin{aligned} \hat{y}_{k,k-1} &= \sum_{i=0}^{2L} \eta_i^m \psi_{k,k-1}^{(i)} \\ P_k^{yy} &= R_k + \sum_{i=0}^{2L} \eta_i^c \left(\psi_{k,k-1}^{(i)} - \hat{y}_{k,k-1} \right) \left(\psi_{k,k-1}^{(i)} - \hat{y}_{k,k-1} \right)^T \\ P_k^{xy} &= \sum_{i=0}^{2L} \eta_i^c \left(\chi_{k,k-1}^{(i)} - \hat{x}_{k,k-1} \right) \left(\psi_{k,k-1}^{(i)} - \hat{y}_{k,k-1} \right)^T \end{aligned} \quad (23)$$

Due to the additive noise assumption, R is added to the output covariance matrix. For calculating the Kalman gain matrix K , covariance matrices are used, using:

$$K_k = P_k^{xy} \left(P_k^{yy} \right)^{-1} \quad (24)$$

And then this Kalman gain matrix is used to update covariance estimates and the state, as in:

$$\begin{aligned} \hat{x}_k &= \hat{x}_{k,k-1} + K_k \left(y_k - \hat{y}_{k,k-1} \right) \\ P_k &= P_{k,k-1} - K_k P_k^{yy} K_k^T \end{aligned} \quad (25)$$

With y_k , the measurement vector, \hat{x}_k is the a posteriori state and P_k is the covariance estimates.

3.3 The moving horizon estimation

The moving horizon estimation is a powerful means of estimating the states, and having in particular the possibility to constrain the outputs, states and noises. We can be described it as a least-squares optimization that leads to a states' estimation and working with a limited amount of information. Its particularity is to avoid the recursive manner characteristic of the extended Kalman filter. Under different approaches, several researchers [22–28] studied it, however presenting many similarities. The moving and full state estimations almost follow the same steps. In the moving state estimation, variables can be handled contrary to the full state estimation. In the full state estimation, at current time k , all variables from initial time $n = 0$ to $n = k$ are used in the calculation. With a horizon H , the moving state estimation uses in the calculation only the concerned variables (measured outputs,

manipulated inputs and estimated states) from $n = k + 1 - H$ to $n = k$, a moving vectors collect them. First of all, consider the full state estimation problem. Let assume that the process can be represented by the following continuous-time model [29–31]:

$$\dot{x}(t) = f(x(t), u(t)) + Gw(t) \quad (26)$$

where w_k is the control noise.

Where the Gaussian noise of zero mean is w . We can describe the measured outputs y by the discrete-time model

$$y_k = h(x_k) + v_k \quad (27)$$

where v_k is the observation noise.

The equivalent linear discrete model is given by:

$$x_{k+1} = Ax_k + Bu_k + Gw_k \quad (28)$$

where the matrices A and B are the Jacobian matrices with respect to f in relation to x_k and u_k , respectively. The measurement model is linearized as:

$$y_{k+1} = Cx_{k+1} + v_{k+1} \quad (29)$$

where the matrix C is the Jacobian matrix of h with respect to x_k . In the full state estimation problem, we have to minimize the following criterion with respect to the sequence of noises $\{w_0, \dots, w_{k-1}\}$ and to the initial state x_0 , and then the states \hat{x}_i are obtained by using Eq. (28).

$$J_k = (x_0 - \hat{x}_0)^T \Pi_0^{-1} (x_0 - \hat{x}_0) + \sum_{i=0}^{k-1} (v_{i+1}^T R^{-1} v_{i+1} + w_i^T Q^{-1} w_i) \quad (30)$$

The weighting matrices Π_0^{-1} , Q^{-1} and R^{-1} , respectively, symbolize the initial estimation, the confidence in the dynamic model and the measurements. The main disadvantage of full state estimation is that during the computation we notice the size of the optimization problem grows as time increases, and would likely cause a failure in the optimization. The favorable solution to this increasing size is to set the problem according to a moving-horizon approach.

Let us consider the problem of moving state estimation. The criterion Eq. (30) is split into two parts [24, 25]:

$$J_k = J_{k-H} + \sum_{i=k-H}^{k-1} (v_{i+1}^T R^{-1} v_{i+1} + w_i^T Q^{-1} w_i) = J_{k-H} + J^{mhe} \quad (31)$$

The second term J^{mhe} of the criterion Eq. (31) depends on the sequence of noises $\{w_{k-H}, \dots, w_{k-1}\}$ and on the state x_{k-H} . Assume that $k > H$ and set the optimized criterion:

$$J_{k-H}^* = \min_{x_0, w_0, \dots, w_{k-H-1}} J_{k-H} \quad (32)$$

And then, in the full optimized criterion becomes:

$$J_k^* = \min_{x_0, w_0, \dots, w_{k-1}} J_k \quad (33)$$

$$= \min_{z, w_{k-H}, \dots, w_{k-1}} \left[\sum_{i=k-H}^{k-1} (v_{i+1}^T R^{-1} v_{i+1} + w_i^T Q^{-1} w_i) \right] + J_{k-H}^*(z) \quad (34)$$

where z is the arrival state x_{k-H} based on the optimized variables $\{w_{k-H}^*, \dots, w_{k-H-1}^*\}$ and x_0 .

In practice, it is very complicated and almost impossible to really minimize $J_{k-H}(z)$ when k becomes large enough as this would be a full estimation problem again. The recommend solution is to retain the previous values of the optimized criterion J_k^* obtained by moving horizon estimation denoted by $J_k^{mhe}(z)$ along time k and to approximate $J_{k-H}(z)$ as:

$$J_{k-H}(z) \approx (z - \hat{x}_{k-H}^{mhe})^T \Pi_{k-H}^{-1} (z - \hat{x}_{k-H}^{mhe}) + J_{k-H}^{mhe}(z) \quad (35)$$

where \hat{x}_{k-H}^{mhe} is the state estimated by moving horizon observer at time $(k-H)$. Under these assumptions, the criterion Eq. (31) becomes:

$$J_k = \sum_{i=k-H}^{k-1} (v_{i+1}^T R^{-1} v_{i+1} + w_i^T Q^{-1} w_i) + (z - \hat{x}_{k-H}^{mhe})^T \Pi_{k-H}^{-1} (z - \hat{x}_{k-H}^{mhe}) + J_{k-H}^{mhe}(z) \quad (36)$$

The discrete Riccati equation we used for the covariance matrix of the Kalman filter is called to update Π_k :

$$\Pi_k = A \Pi_{k-1} A^T + G Q G^T - A \Pi_{k-1} C^T [C \Pi_{k-1} C^T + R]^{-1} C \Pi_{k-1} A^T \quad (37)$$

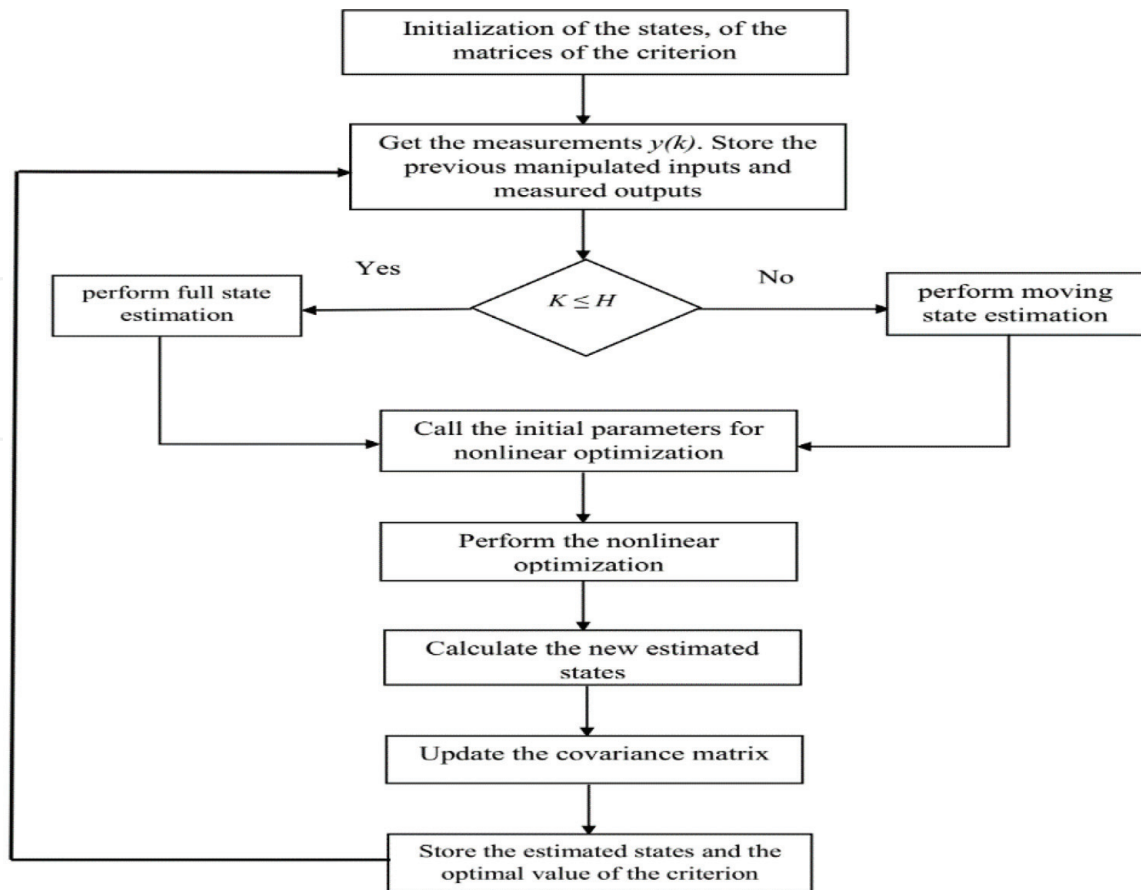


Figure 2.
 Moving horizon estimation algorithm.

With Π_0 given. The Moving horizon estimation algorithm is described by the diagram in **Figure 2**.

4. Numerical results

In this section, the performances of the proposed observers are illustrated in simulation. Observers' algorithms have been implemented in MATLAB/SIMULINK software. The doubly-fed induction generator system states which have been used for estimation are expressed into a vector x , this vector includes as parameters to estimate the stator and rotor resistances, as follows:

$$x = [\Phi_{ds} \quad \Phi_{qs} \quad \Phi_{dr} \quad \Phi_{qr} \quad R_s \quad R_r]^T \quad (38)$$

The inputs of the system are the rotor angular electrical speed, stator and rotor voltages, as in:

$$u = [v_{ds} \quad v_{qs} \quad v_{dr} \quad v_{qr} \quad \omega_r]^T \quad (39)$$

The d and q axis of stator and rotor currents and the mechanical torque constitute the measurements of the systems,

$$y = [T_m \quad i_{ds} \quad i_{qs} \quad i_{dr} \quad i_{qr}]^T \quad (40)$$

Table 3 shows a comparison of the running time of high gain observer (HGO), the unscented Kalman filter (UKF), and the moving horizon estimation (MHE) for the DFIG system. The high gain observer being the fastest among the three methods under various modes especially the healthy mode which represents a healthy DFIG and the faulty mode where stator and rotor resistance would have changed value during the operation of the DFIG. **Tables 4** and **5** give the parameters of UKF and MHE only. For the UKF, the primary, secondary, and tertiary scaling parameters α , β and κ are chosen as 1, 2, and 0, respectively.

	HGO	UKF	MHE
Healthy mode	1.200	1.190	152.978
Faulty mode	1.901	1.666	154.234

Table 3.
Running time of the three observers for the DFIG (in seconds).

Parameters	Values
Weight matrix G	eye(6)
Covariance matrix P ₀	3eye(6)
Covariance matrix Q	0.5eye(6)
Covariance matrix R	eye(5)
Length horizon H	10
Initial guess	[0; 0.5; 0.5; 1; 0.02; 0.02]

Table 4.
MHE parameters.

Parameters	Values
Covariance matrix P_0	eye(6)
Covariance matrix Q	$10^{-2}\text{diag}([111110-410-4])$
Covariance matrix R	$10^{-2}\text{diag}([111111])$
Initial guess	[0; 0.5; 0.5; 1; 0.02; 0.02]

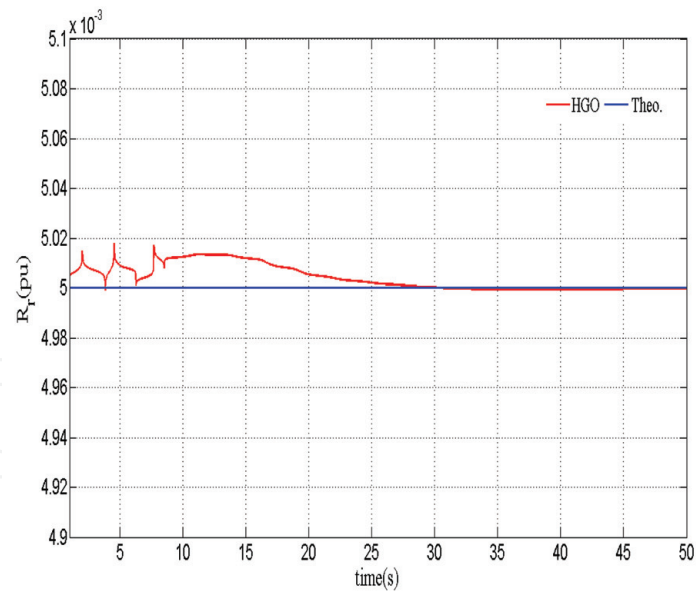
Table 5.
 UKF parameters.

Figures 3 and **4** show the generated estimates of the rotor and stator resistances by the HGO, UKF and the MHE in the healthy mode of working of the DFIG. Nevertheless, **Figures 5** and **6** show the generated estimates of the rotor and stator resistances by the HGO, UKF and the MHE in the faulty mode of working, let us mention that faulty mode is simply a mode where the DFIG undergoes a fault on its stator and/or rotor resistances during the operation. We just simulated those scenarios to appreciate the estimation performance of different observers in particular the HGO, UKF and MHE for process monitoring or diagnostics purposes. We can observe that the estimates by the MHE converges to the actual parameters in fewer time compared to the HGO and UKF. In **Table 3**, we notice the total computation time to obtain an estimate for the HGO algorithm is about 1.200 seconds, for the UKF algorithm is also about 1.190 seconds while the MHE algorithm took 152.978 seconds to estimate the parameters in the normal mode of working, and in the faulty mode, we have about 1.901, 1.666 and 154.234 seconds for those observers, respectively. We can conclude that when the asynchronous machine has a stator or rotor resistance fault, the estimation time increases. The reason the MHE algorithm takes longer to make an estimate is that in simulation, the optimization of the objective function, through a nonlinear programming algorithm has been performed at each time step, in this case study the nonlinear programming algorithm used is the sequential quadratic programming in the MATLAB in-built function *fmincon*. For the HGO we can underline this, a big value of θ leads to consolidate the linear part and to guarantee the stability of the nonlinear part through the fact that φ is imposed globally Lipschitz in relation to x [27]. If θ are big enough, the time of convergence decreases, but the observation becomes extremely sensitive to the measurement noises. A small value of θ leads to the reverse effect obviously. In comparison with the extended Kalman filter, this observer contains a lot less of setting variables that facilitates its optimization. Besides the number of equations to solve are a lot weaker and it decreases the time of calculation considerably. To know that the number of differential equations to solve for the Kalman filter is of $n + \frac{n(n+1)}{2}$ such as, n is the size of observation vector, when that number is n for the high gain observer [18], for our experiment the value of the gain is $\theta = 27$, on the other hand, the UKF algorithm has to handle.

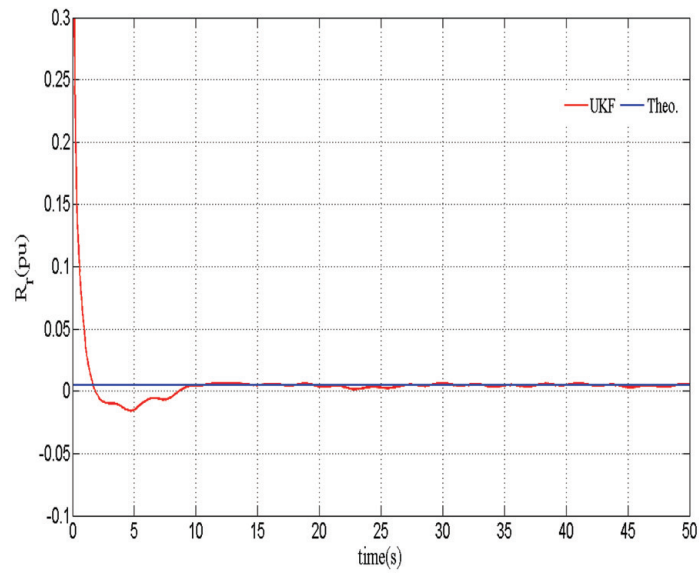
$2L + 1$ sigma points and associated weights to represent state of the system. **Tables 6** and **7** show the standard deviation and the variance of the estimation error. The comparison of these observers can be made by finding the mean squared error (MSE) value. The MSE can be evaluated as:

$$MSE = \frac{1}{N \times n} \sum_{i=1}^N (\theta_i - \hat{\theta}_i)^2 \quad (41)$$

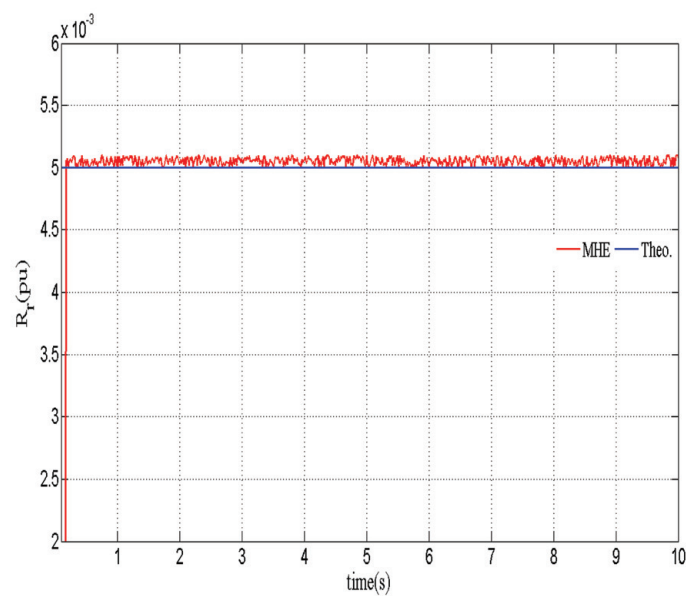
where N is the number of time steps, n is the dimension of state vector, θ_i is the simulated value and $\hat{\theta}_i$ is the estimated value from the filters. **Table 8** shows a comparison of the three observers by finding the mean squared error in the healthy



(a)

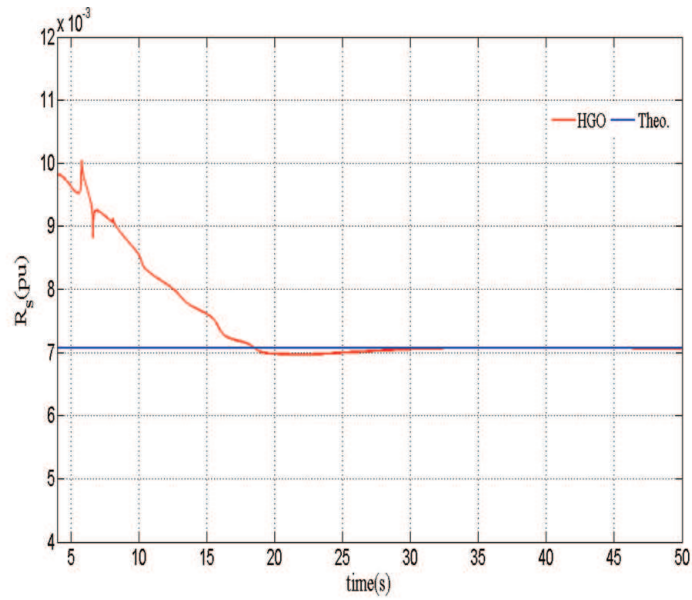


(b)

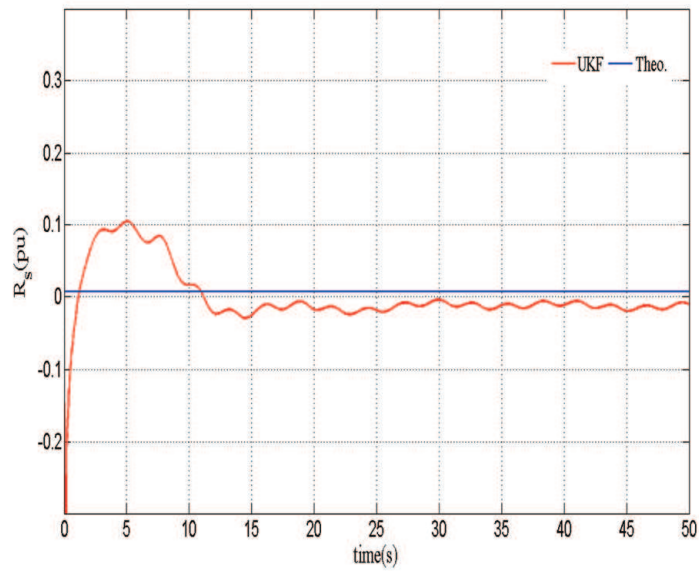


(c)

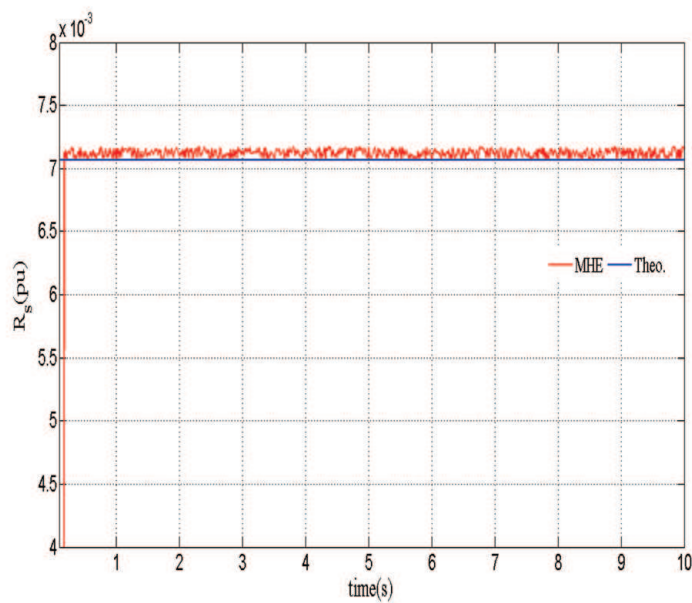
Figure 3. Rotor resistance estimation in a healthy mode with HGO, UKF and MHE. (a) Rotor resistance estimation (HGO), (b) Rotor resistance estimation (UKF), (c) Rotor resistance estimation (MHE).



(a)

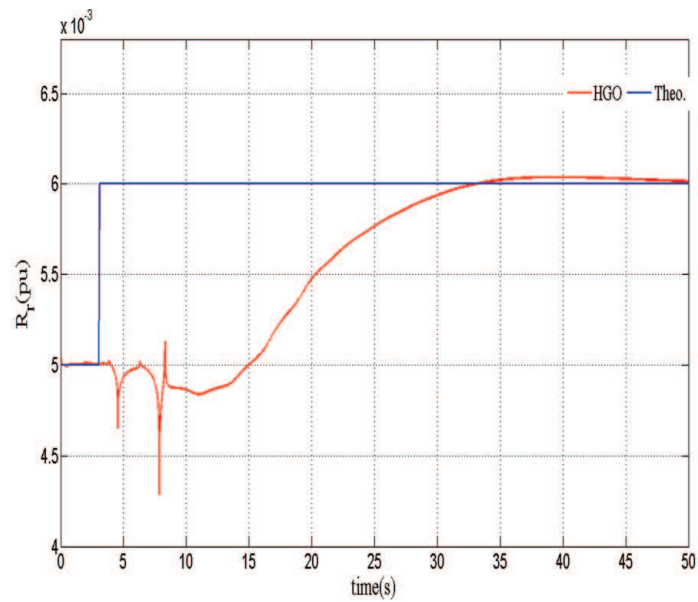


(b)

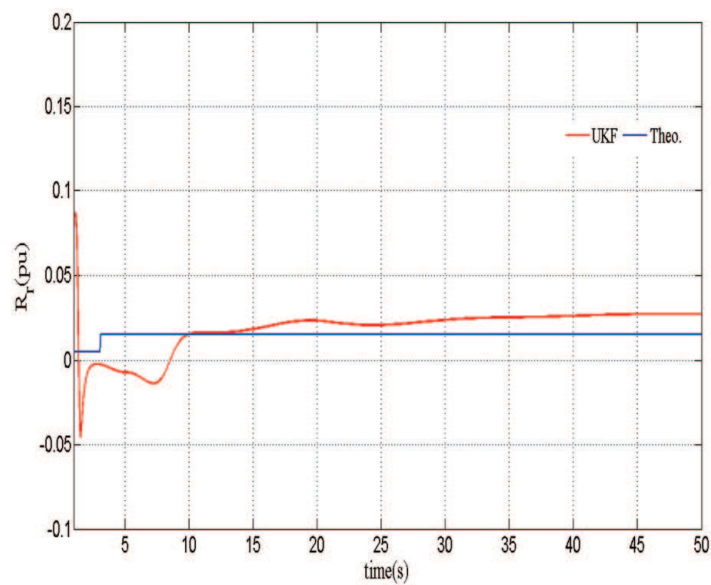


(c)

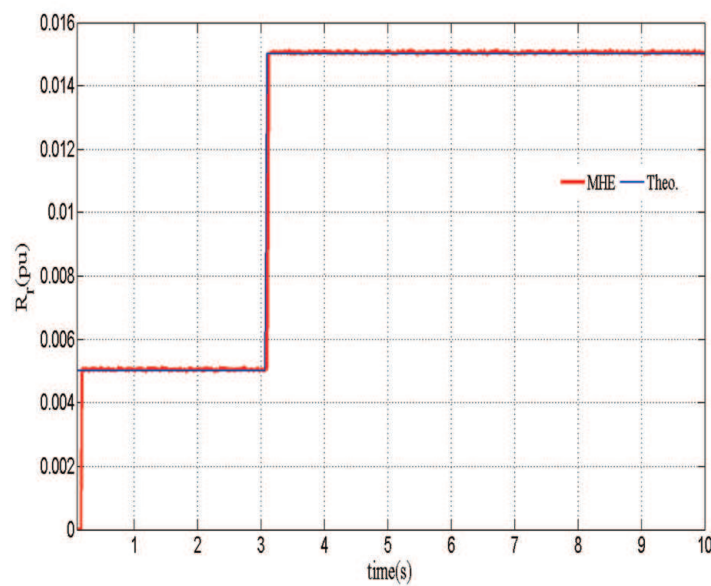
Figure 4. Stator resistance estimation in a healthy mode with HGO, UKF and MHE. (a) Stator resistance estimation (HGO), (b) Stator resistance estimation (UKF), (c) Stator resistance estimation (MHE).



(a)

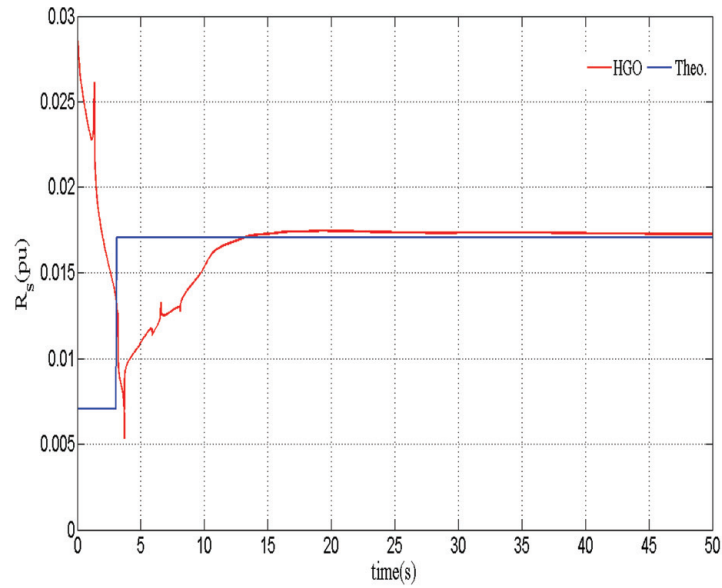


(b)

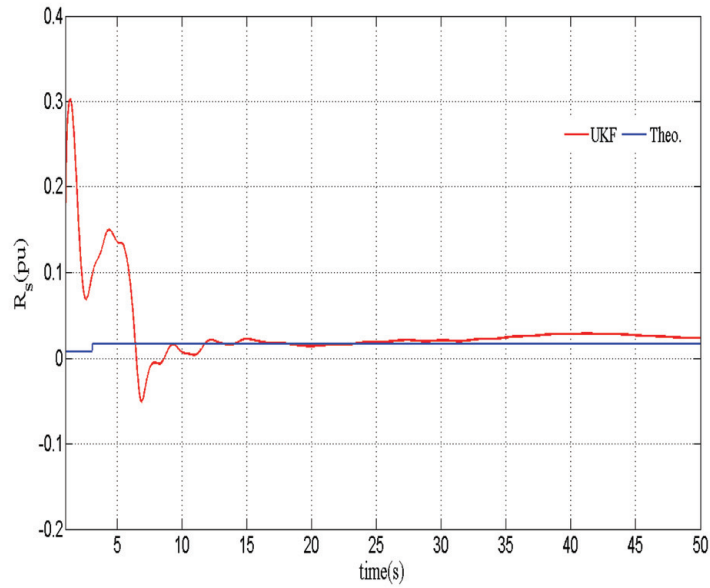


(c)

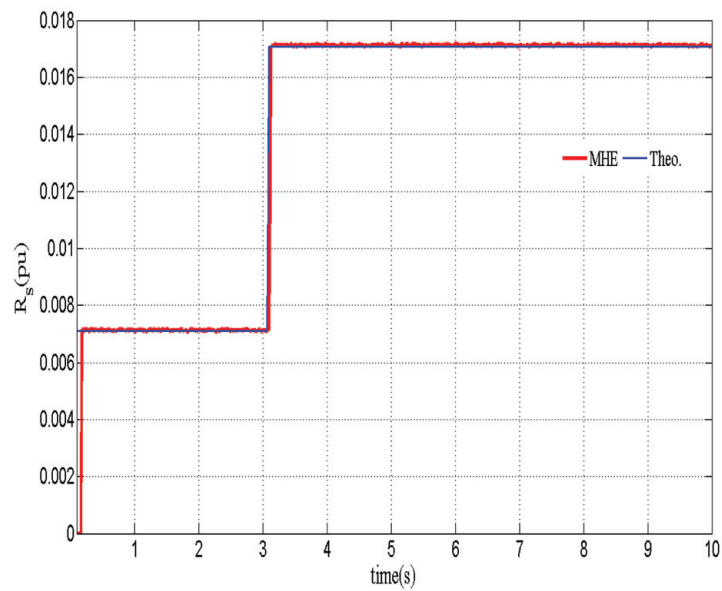
Figure 5. Rotor resistance estimation in a faulty mode with HGO, UKF and MHE. (a) Rotor resistance estimation (HGO), (b) Rotor resistance estimation (UKF), (c) Rotor resistance estimation (MHE).



(a)



(b)



(c)

Figure 6. Stator resistance estimation in a faulty mode with HGO, UKF and MHE. (a) Stator resistance estimation (HGO), (b) Rotor resistance estimation (UKF), (c) Rotor resistance estimation (MHE).

	Std (HGO) $\times 10^{-5}$	Std (UKF) $\times 10^{-5}$	Std (MHE) $\times 10^{-5}$
Rs	350	7450	57.75
Rr	7.29	3940	41.38
	Variance (HGO) $\times 10^{-5}$	Variance (UKF) $\times 10^{-5}$	Variance (MHE) $\times 10^{-5}$
Rs	1.26	550	0.033
Rr	0.0053	160	0.017

Table 6.
General statistics of the three observers (healthy mode).

	Std (HGO) $\times 10^{-4}$	Std (UKF) $\times 10^{-4}$	Std (MHE) $\times 10^{-4}$
Rs	25	8208	270
Rr	4.86	278	26
	Variance (HGO) $\times 10^{-5}$	Variance (UKF) $\times 10^{-5}$	Variance (MHE) $\times 10^{-5}$
Rs	0.62	6737	0.74
Rr	0.024	77.47	0.702

Table 7.
General statistics of the three observers (faulty mode).

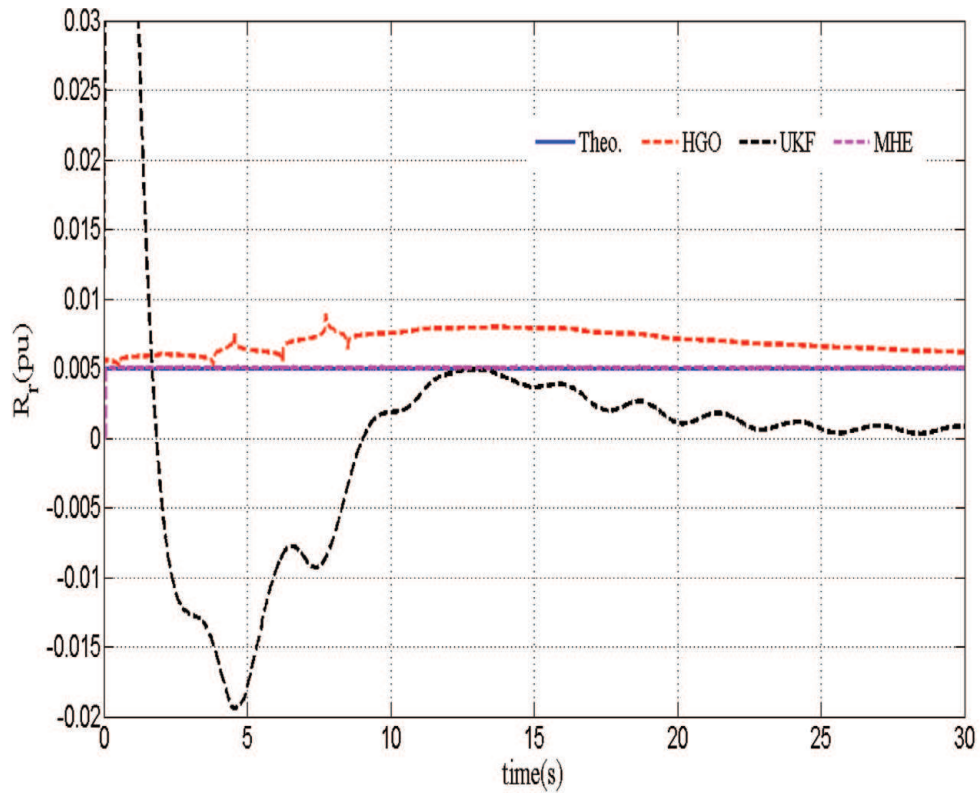
	HGO		UKF		MHE	
	Healthy	Faulty	Healthy	Faulty	Healthy	Faulty
Rs	4.73E-06	8.02E-06	8.66E-04	9.65E-04	1.11E-07	1.27E-07
Rr	1.77E-09	1.79E-05	9.36E-05	1.14E-04	5.71E-08	7.33E-08
Φ_{ds}	5.70E-04	6.31E-04	9.02E-05	9.23E-05	21.0E-04	11.0E-04
Φ_{qs}	1.93E-06	2.10E-06	1.10E-16	1.10E-16	39.0E-04	27.0E-04
Φ_{dr}	2.08E-08	16.00E-04	6.47E-06	6.87E-06	246E-04	210E-04
Φ_{qr}	1.73E-10	4.81E-06	1.10E-06	1.10E-06	67.0E-04	70.0E-04

Table 8.
MSE values of nonlinear observers: HGO, UKF and MHE are compared.

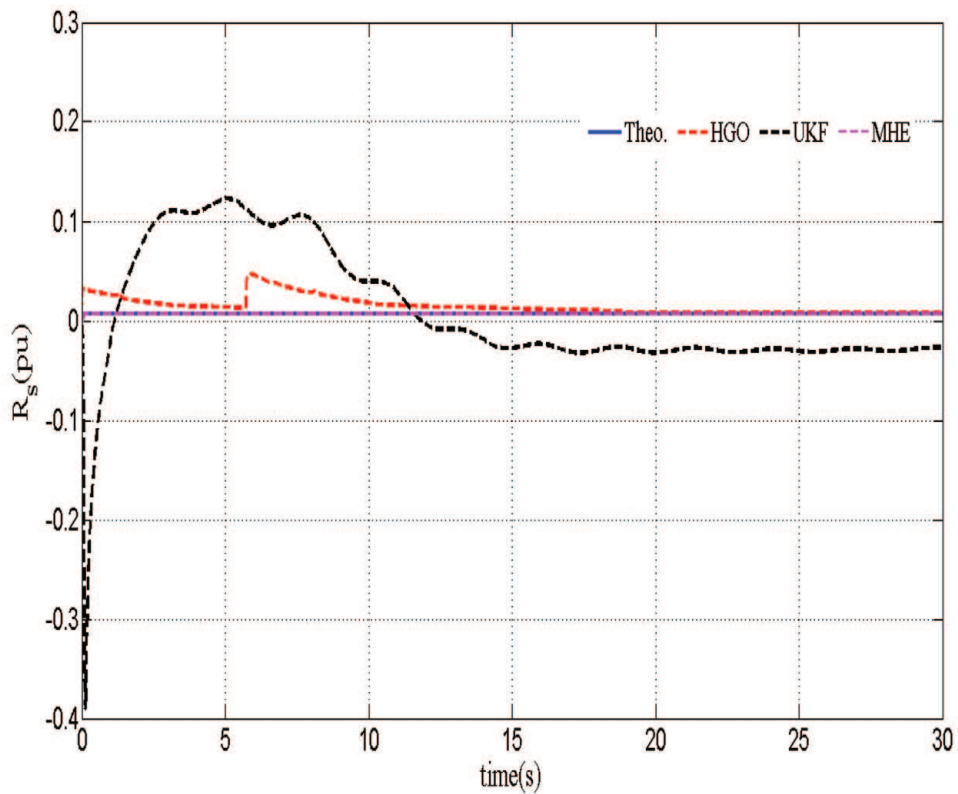
and the faulty mode of operation of the DFIG and we can notice that generally, the mean squared error of states and parameters in faulty mode is relatively greater than those in the healthy mode because of the fault occurring suddenly during the operation, but we can always see the high performance of the moving horizon estimation on the others observers.

To verify the robustness, we have performed parametric variation on the observer in relation to the identified values. **Figures 7 and 8** show the responses obtained when a rotor inductance variation of +50 and -50% is considered for the observer test. The robustness of the observers' scheme with respect to this parameter changes is clearly shown. In **Figures 7 and 8**, it is clearly shown that a +50 and -50% rotor inductance variation generates a high statistical difference on rotor and stator resistances for the unscented Kalman filter. For the high gain observer, that variation is much more felt on the rotor resistance on the both figures. Incontestably the moving horizon estimation seems remain insensitive to the parametric

variations but it is not so, it is just that the statistical difference generated is weak enough compared to others. From these responses, we can conclude that the rotor inductance changes do not affect the performance of the moving horizon estimation



(a)



(b)

Figure 7. Robustness test. Rotor inductance variation (+50%). (a) Rotor resistance estimation, (b) Stator resistance estimation.

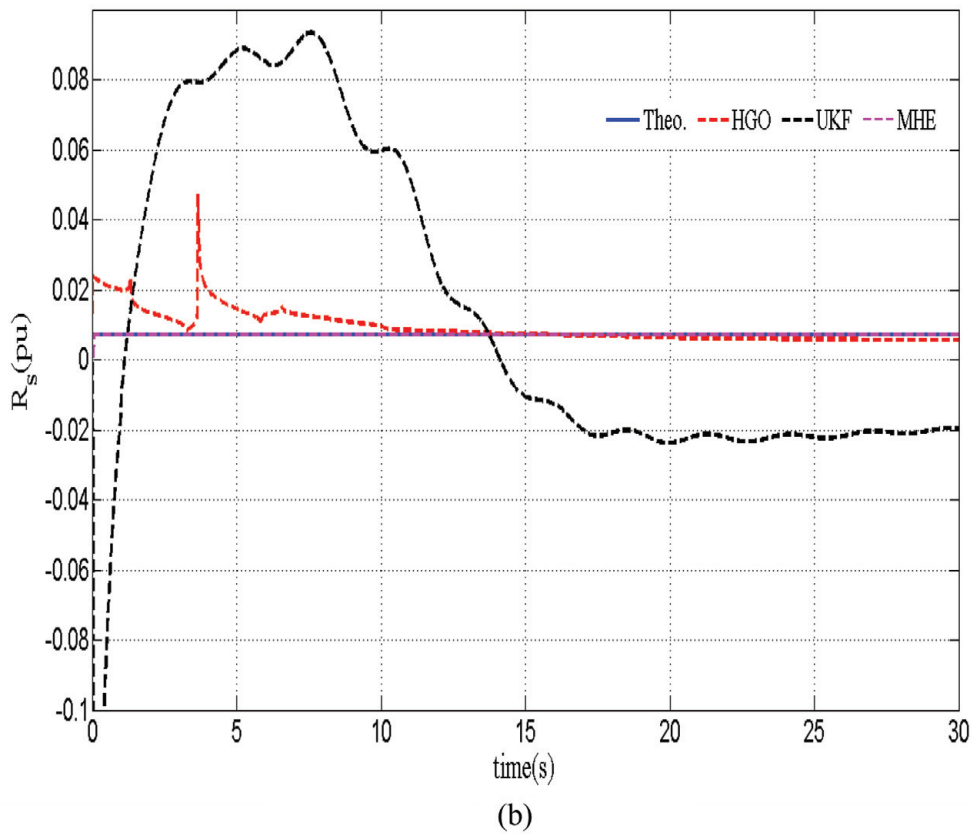
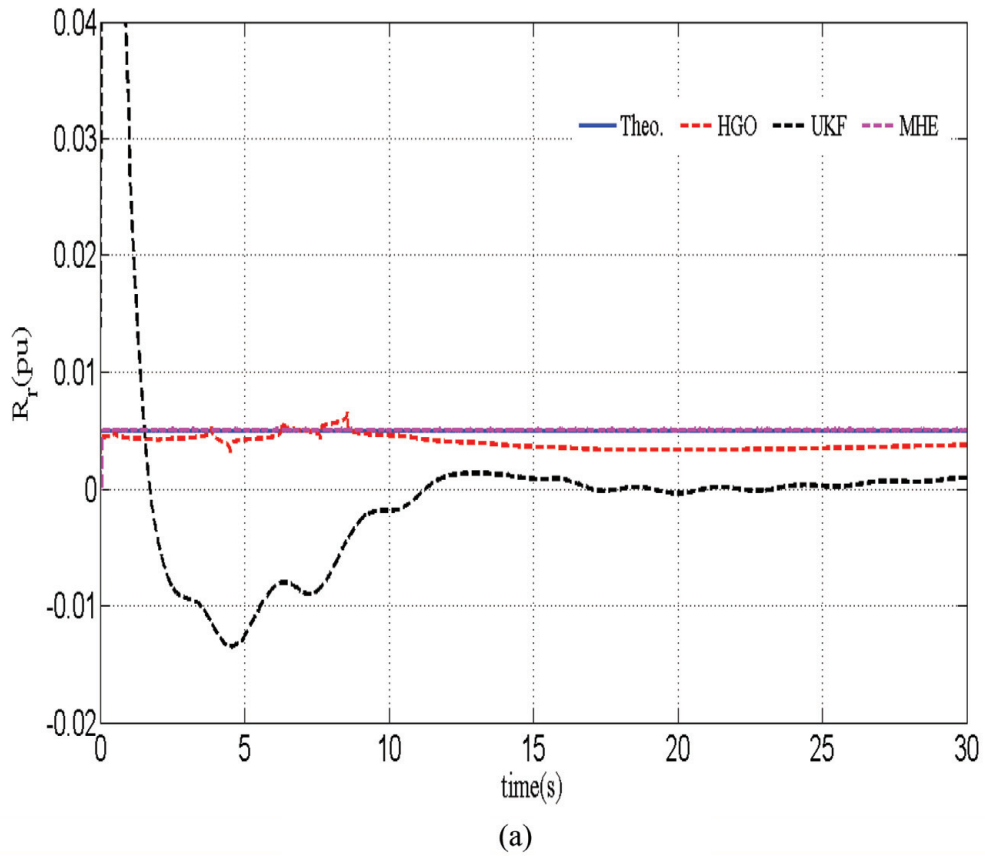


Figure 8. Robustness test. Rotor inductance variation (-50%). (a) Rotor resistance estimation, (b) Stator resistance estimation.

considerably, but in regard to the other observers, the changes disturb their performance a lot as shown in the figures and that the MHE scheme is robust enough under parametric uncertainties.

5. Conclusion

In this chapter, a general framework for the doubly fed induction generator has been presented in order to carry out a dynamic estimation of states and parameters of the DFIG. The DFIG parameters are largely influenced by different factors (for instance, temperature, magnetic saturation and eddy current) that is why it is necessary to develop techniques to estimate the changes of parameters. The proposed techniques are performed with high gain observer (HGO), unscented Kalman filter (UKF) and moving horizon estimation algorithms using noisy measurements. A comparison of the three estimation techniques has been made under different aspects notably, computation time and estimation accuracy, in two modes of operation of the DFIG, the healthy mode and the faulty mode. The MHE estimation technique has significantly lower estimation error and converges with fewer samples time than the HGO and the UKF. Whatever the mode of functioning, the simulation results showed that a good standard of performance could be obtained even in the presence of measurement noise.


IntechOpen

Author details

Steve Alan Talla Ouambo, Alexandre Teplaira Boum*
and Adolphe Moukengue Imano
Department of Physics, Faculty of Science, University of Douala, Cameroon

*Address all correspondence to: boumat2002@yahoo.fr

IntechOpen

© 2019 The Author(s). Licensee IntechOpen. This chapter is distributed under the terms of the Creative Commons Attribution License (<http://creativecommons.org/licenses/by/3.0>), which permits unrestricted use, distribution, and reproduction in any medium, provided the original work is properly cited. 

References

- [1] Tazil M, Kumar V, Bansal RC, Kong S, Dong ZY, Freitas W, et al. Three-phase doubly fed induction generators: An overview. *IET Electric Power Applications*. 2010;4(2):75-89
- [2] Marinelli M, Morini A, Pitto A, Federico S. Modeling of doubly fed induction generator (DFIG) equipped wind turbine for dynamic studies. In: 2008 43rd International Universities Power Engineering Conference. Padova, Italy: IEEE; 2008. pp. 1-6
- [3] Shenglong Y, Emami K, Fernando T, Herbert HCI, Wong KP. State estimation of doubly fed induction generator wind turbine in complex power systems. *IEEE Transactions on Power Systems*. 2016;31(6):4935-4944
- [4] Pena R, Clare JC, Asher GM. Doubly fed induction generator using back-to-back PWM converters and its application to variable-speed wind-energy generation. *IEE Proceedings-Electric Power Applications*. 1996; 143(3):231-241
- [5] Ledesma P, Usaola J. Doubly fed induction generator model for transient stability analysis. *IEEE Transactions on Energy Conversion*. 2005;20(2):388-397
- [6] Rothenhagen K, Fuchs FW. Current sensor fault detection and reconfiguration for a doubly fed induction generator. In: 2007 IEEE Power Electronics Specialists Conference. Orlando: IEEE; 2007. pp. 2732-2738
- [7] Campos-Delgado DU, Espinoza-Trejo DR, Palacios E. Fault-tolerant control in variable speed drives: A survey. *IET Electric Power Applications*. 2008;2(2):121-134
- [8] Abdelmalek S, Rezazi S, Azar AT. Sensor faults detection and estimation for a dfig equipped wind turbine. *Energy Procedia*. 2017;139:3-9
- [9] Rothenhagen K, Fuchs FW. Model-based fault detection of gain and offset faults in doubly fed induction generators. In: 2009 IEEE International Symposium on Diagnostics for Electric Machines, Power Electronics and Drives. Cargese: IEEE; 2009. pp. 1-6
- [10] Li D, Lin X, Hu S, Kang Y. An adaptive estimation method for parameters of doubly-fed induction generators (DFIG) in wind power controller. In: 2010 Asia-Pacific Power and Energy Engineering Conference. Chengdu: IEEE; 2010. pp. 1-4
- [11] Julier SJ, Jeffrey KU. New extension of the Kalman filter to nonlinear systems. In: *Signal Processing, Sensor Fusion, and Target Recognition VI*. Vol. 3068. International Society for Optics and Photonics; 1997. pp. 182-194
- [12] Wan EA, Van Der Merwe R. The unscented Kalman filter for nonlinear estimation. In: *Proceedings of the IEEE 2000 Adaptive Systems for Signal Processing, Communications, and Control Symposium*. IEEE; 2000. pp. 153-158
- [13] Dida A, Attous DB. Doubly-fed induction generator drive based WECS using fuzzy logic controller. *Frontiers in Energy*. 2015;9(3):272-281
- [14] Pan X, Ju P, Wu F, Jin Y. Hierarchical parameter estimation of DFIG and drive train system in a wind turbine generator. *Frontiers of Mechanical Engineering*. 2017;12(3): 367-376
- [15] Heier S. Grid integration of wind energy: onshore and offshore conversion systems. John Wiley & Sons; 2014. pp. 31-117

- [16] Leonhard W. Controlled ac drives, a successful transition from ideas to industrial practice. *Control Engineering Practice*. 1996;**4**(7):897-908
- [17] Yang L, Xu Z, Østergaard J, Dong ZY, Wong KP, Ma X. Oscillatory stability and eigenvalue sensitivity analysis of a DFIG wind turbine system. *IEEE Transactions on Energy Conversion*. 2011;**26**(1):328-339
- [18] Boum AT, Talla SA. High gain observer and moving horizon estimation for parameters estimation and fault detection of an induction machine: A comparative study. *Journal of Control and Instrumentation*. 2017;**15-26**(08):8
- [19] Nijmeijer H, Fossen TI. *New Directions in Nonlinear Observer Design*. Vol. 244. Springer; 1999
- [20] Bornard G, Hammouri H. A high gain observer for a class of uniformly observable systems. In: *Proceedings of the 30th IEEE Conference on Decision and Control*. Brighton, UK: IEEE; 1991. pp. 1494-1496
- [21] Rhudy M, Gu Y. Understanding nonlinear Kalman filters. Part II: An implementation guide. *Interactive Robotics Letters*; 2013. p. 1-18
- [22] Corriou J-P. *Process Control*. Springer-Verlag; 2004
- [23] Michalska H, Mayne DQ. Moving horizon observers and observer-based control. *IEEE Transactions on Automatic Control*. 1995;**40**(6): 995-1006
- [24] Rao CV, Rawlings JB, Lee JH. Constrained linear state estimation—A moving horizon approach. *Automatica*. 2001;**37**(10):1619-1628
- [25] Robertson DG, Lee JH, Rawlings JB. A moving horizon-based approach for least-squares estimation. *AIChE Journal*. 1996;**42**(8):2209-2224
- [26] Slotine J-JE, Hedrick JK, Misawa EA. On sliding observers for nonlinear systems. *Journal of Dynamic Systems, Measurement, and Control*. 1987; **109**(3):245-252
- [27] Gauthier JP, Hammouri H, Othman S. A simple observer for nonlinear systems applications to bioreactors. *IEEE Transactions on Automatic Control*. 1992;**37**(6):1875
- [28] Choqueuse V, Benbouzid M. Induction machine faults detection using stator current parametric spectral estimation. *Mechanical Systems and Signal Processing*. 2015;**52**:447-464
- [29] Liu K, Zhu ZQ. Position offset-based parameter estimation for permanent magnet synchronous machines under variable speed control. *IEEE Transactions on Power Electronics*. 2015;**30**(6):3438-3446
- [30] Smith AN, Gadoue SM, Finch JW. Improved rotor flux estimation at low speeds for torque MRAS-based sensorless induction motor drives. *IEEE Transactions on Energy Conversion*. 2016;**31**(1):270-282
- [31] Alonge F, Cirrincione M, Pucci M, Sferlazza A. Input-output feedback linearization control with on-line MRAS-based inductor resistance estimation of linear induction motors including the dynamic end effects. *IEEE Transactions on Industry Applications*. 2016;**52**(1):254-266